Applied Soft Computing 47 (2016) 332–342

Contents lists available at ScienceDirect

Applied Soft Computing

journal homepage: www.elsevier.com/locate/asoc

Multi-objective optimization of expensive electromagnetic simulation models

Slawomir Koziel [a,b,*], Adrian Bekasiewicz [a,b]

[a] School of Science and Engineering, Reykjavik University, 101 Reykjavik, Iceland
[b] Faculty of Electronics, Telecommunications and Informatics, Gdansk University of Technology, 80-233 Gdansk, Poland

ARTICLE INFO

Article history:
Received 30 June 2015
Received in revised form 30 March 2016
Accepted 24 May 2016
Available online 18 June 2016

Keywords:
Computer-aided design (CAD)
Computational electromagnetics
Electromagnetic (EM)-simulation models
Simulation-driven design
Multi-objective optimization
Surrogate modeling
Evolutionary algorithms
Space mapping

ABSTRACT

Vast majority of practical engineering design problems require simultaneous handling of several criteria. For the sake of simplicity and through a priori preference articulation one can turn many design tasks into single-objective problems that can be handled using conventional numerical optimization routines. However, in some situations, acquiring comprehensive knowledge about the system at hand, in particular, about possible trade-offs between conflicting objectives may be necessary. This calls for multi-objective optimization that aims at identifying a set of alternative, Pareto-optimal designs. The most popular solution approaches include population-based metaheuristics. Unfortunately, such methods are not practical for problems involving expensive computational models. This is particularly the case for microwave and antenna engineering where design reliability requires utilization of CPU-intensive electromagnetic (EM) analysis. In this work, we discuss methodologies for expedited multi-objective design optimization of expensive EM simulation models. The solution approaches that we present here rely on surrogate-based optimization (SBO) paradigm, where the design speedup is obtained by shifting the optimization burden into a cheap replacement model (the surrogate). The latter is utilized for generating the initial approximation of the Pareto front representation as well as further front refinement (to elevate it to the high-fidelity EM simulation model level). We demonstrate several application case studies, including a wideband matching transformer, a dielectric resonator antenna and an ultra-wideband monopole antenna. Dimensionality of the design spaces in the considered examples vary from six to fifteen, and the design optimization cost is about one hundred of high-fidelity EM simulations of the respective structure, which is extremely low given the problem complexity.

1. Introduction

Electromagnetic (EM)-simulation models are nowadays ubiquitous in various fields such as RF and microwave engineering [1], antenna design [2], photonics [3], design of wireless power transfer systems [4], microwave imaging [5], non-destructive testing [6], to name just a few. High-fidelity EM analysis permits accurate evaluation of the system performance, however, it might be computationally expensive, particularly for complex structures. In many situations, computational models have to account not just for the structure under design but also its environment that the system is electromagnetically coupled with, and which affects its operation [7,8]. As a matter of fact, EM simulation might be the only reliable way of estimating the system performance with the simplified (e.g., analytical) models either not available or being very inaccurate.

High cost of high-fidelity EM analysis becomes a fundamental bottleneck from the simulation-driven design point of view, especially design automation through numerical optimization. While relatively simple EM models of individual components (filters, antennas, couplers, etc.) simulate in a few minutes per design, more complex structures (antenna arrays, electrically large structures, components simulated with their environment such as on-vehicle antennas, integrated photonic devices) require a few hours up to many days for simulation. Conventional optimization algorithms (both gradient-based [9] and derivative-free [10], particularly population-based metaheuristics such as evolutionary algorithms [11], particle swarm optimizers [12] or differential evolution [13]) require large number of objective function evaluations to converge, which is often computationally prohibitive. Consequently, the most popular approaches to simulation-driven design

* Corresponding author at: School of Science and Engineering, Reykjavik University, 101 Reykjavik, Iceland.
E-mail addresses: koziel@ru.is (S. Koziel), bekasiewicz@ru.is (A. Bekasiewicz).

http://dx.doi.org/10.1016/j.asoc.2016.05.033
1568-4946/

are hand-on procedures involving heavy interactions with the designer [14,15]. A notable example is design through parameter sweeps (usually, one parameter at a time), guided by engineering experience. Such methods, although laborious, typically lead to acceptable (yet not optimum) results in reasonable timeframe when executed by skilled engineers with sufficient background and experience in solving a particular class of design tasks.

Clearly, automated design optimization is highly desirable. Adjoint sensitivity [16,17] is one of technologies that allow speeding up EM-driven optimization process [18,19] by providing information about the system response and its gradients at little extra computational cost. Unfortunately, this technology is not yet widely used in computational electromagnetic community and commercially only available through a few EM solvers [20,21]. One of the most promising approaches to computationally efficient simulation-driven design is surrogate-based optimization (SBO) [22,23]. In SBO, direct optimization of the expensive simulation model is replaced by iterative construction and re-optimization of its cheap representation, referred to as a surrogate [22]. Various SBO techniques mostly differ in the way the surrogate model is constructed. A comprehensive review of surrogate-based techniques for solving expensive real-world problems can be found in [24]. In [25] a survey of surrogate-assisted optimization from the perspective of evolutionary computation is presented.

The methods exploiting data-driven (approximation) surrogates are usually used for global optimization (EGO-type methods [26,27], artificial neural networks [42], or SAEA algorithms [28,29]), where a surrogate model is constructed from sampled simulation data and subsequently used as a prediction tool for identifying the most promising designs. The surrogate is updated using suitably defined infill points aiming either at improvement of the global accuracy of the model [22] or in exploitation of the promising regions of the design space [22]. Physics-based surrogate models are constructed by suitable correction of the underlying low-fidelity models (such as equivalent circuits [30] or coarse-mesh EM simulation models [7]). The most popular physics-based SBO techniques in computational electromagnetics include space mapping (SM) [31,32], various response correction methods [33–35], feature-based optimization [36], as well as adaptively adjusted design specifications [37]. Because of embedding knowledge about the system at hand, physics-based models normally exhibit better generalization capability than approximation surrogates. On the other hand, due to being relatively expensive, they are better suited for local optimization [7].

Majority of real-world design problems in computational electromagnetics require handling multiple criteria. A typical example that applies particularly to wireless communication systems (especially portable, battery-operated, and wearable devices [38,39]) is design of miniaturized components that still satisfy stringent requirement concerning their electrical performance [7,14,18]. In many cases the design task can be converted into a single-objective optimization problem by appropriate goal prioritization [7]. However, finding possible trade-offs between conflicting objectives may be necessary in certain situations, e.g., to obtain comprehensive information about the capabilities of a given structure/system. This can only be achieved through genuine multi-objective optimization yielding a set of alternative solutions that are Pareto-optimal with respect to given design criteria. Obviously, it leads to additional challenges from the simulation-driven design standpoint.

The most popular multi-objective optimization methods are population-based metaheuristics such as genetic algorithms (GAs) [11,40], or particle swarm optimizers (PSO) [12,41]. Their most important advantage is a capability of finding the entire Pareto set in a single algorithm run. A disadvantage is huge computational cost (normally hundreds, thousands or tens of thousands of objective evaluations) which is computationally prohibitive if the high-fidelity EM simulations are utilized for system evaluation.

Recently, it has been demonstrated that surrogate-based optimization techniques may be extended to handle multi-objective optimization problems in engineering [7,35]. Particular examples of using approximation surrogates for solving real-world problems can be found in [42,43]. In [42], an artificial neural network has been utilized in a combination with a Monte Carlo procedure to accelerate multi-objective design of optical networks by 88% with respect to direct optimization driven by network simulator. Surrogate-based optimization has been also successfully applied for solving multi-objective problems in antenna engineering [43]. Because of relatively high cost of low-fidelity antenna simulations, auxiliary kriging interpolation models have been exploited in [43] to permit feasible Pareto front identification using evolutionary methods.

In this paper, we review the approach introduced in [43] and demonstrate its application—in conjunction with the initial design space reduction—to the design of various types of microwave and antenna components. In particular, we consider examples of miniaturized impedance matching transformer, a dielectric resonator antenna (with three design objectives), and a compact ultra-wideband monopole antenna. Our results indicate that utilization of variable-fidelity EM simulations, approximation modeling, and response correction techniques, allows for identifying Pareto front representations at the cost corresponding to less than a hundred high-fidelity EM simulations of the structures under design. The critical components of the design optimization process, which is an enhancement compared to [43], is utilization of the initial design space reduction. Also, the refinement procedure has been generalized for arbitrary number of objectives. Moreover, we demonstrate that possible imperfections and statistical variability of multi-objective evolutionary optimization of the approximation surrogate (an intermediate step of the design process leading to the initial approximation of the Pareto front) has minor influence on the final Pareto set quality, which is mostly a result of the overall optimization flow arrangement (specifically, operating within a confined region of the design space containing the Pareto front, and surrogate-assisted front refinement procedures).

2. Multi-objective optimization of expensive electromagnetic simulation models

In this section, we briefly outline the procedure for expedited multi-objective optimization of expensive electromagnetic (EM) simulation models. We start by formulating the multi-objective design problem, discuss variable-fidelity EM modeling, describe a simple design space reduction procedure as well as surrogate model construction using kriging interpolation. We also formulate the procedure for generating the initial Pareto-optimal set approximation and its refinement strategy.

2.1. Multi-objective design. Problem formulation

We denote by $\boldsymbol{R}_f(\boldsymbol{x})$ a high-fidelity electromagnetic simulation of the system/structure under design. The response vector $\boldsymbol{R}_f(\boldsymbol{x})$ represent relevant figures of interest, which normally are so-called scattering parameters evaluated over a frequency band of interest [43]. Designable parameters (i.e., structure dimensions) are represented by a vector $\boldsymbol{x}$.

Let $F_k(\boldsymbol{x})$, $k = 1, \ldots, N_{obj}$, be a k-th design objective. A typical situation would be to satisfy minimax-type of specifications such as minimize the reflection coefficient (in particular, to ensure $|S_{11}| \leq -10$ dB in a predefined frequency band, in case of antenna structures [44]). However, other objectives, related to minimiza-

tion of geometry (e.g., maximal lateral size, height, the maximal area of the footprint, volume, etc.) [43].

If $N_{obj} > 1$ then any two designs $\boldsymbol{x}^{(1)}$ and $\boldsymbol{x}^{(2)}$ for which $F_k(\boldsymbol{x}^{(1)}) < F_k(\boldsymbol{x}^{(2)})$ and $F_l(\boldsymbol{x}^{(2)}) < F_l(\boldsymbol{x}^{(1)})$ for at least one pair $k \neq l$, are not commensurable, i.e., none is better than the other in the multi-objective sense. In this case, a Pareto dominance relation $<$ is utilized [11]. We say, for any two designs $\boldsymbol{x}$ and $\boldsymbol{y}$, that $\boldsymbol{x}$ dominates over $\boldsymbol{y}$ ($\boldsymbol{x} < \boldsymbol{y}$) if $F_k(\boldsymbol{x}) \leq F_k(\boldsymbol{y})$ for all $k = 1, \ldots, N_{obj}$, and $F_k(\boldsymbol{x}) < F_k(\boldsymbol{y})$ for at least one k. A goal of multi-objective optimization is to find a representation of a so-called Pareto optimal set X_P composed of the non-dominated designs from the solution space X, such that for any $\boldsymbol{x} \in X_P$, there is no $\boldsymbol{y} \in X$ for which $\boldsymbol{y} < \boldsymbol{x}$ [11].

Thus, our problem can be formulated as follows: given a set of decision variables $\boldsymbol{x}$, our goal is to minimize the objective functions $F_k(\boldsymbol{x})$, under the restrictions defined by the lower and upper bounds for the variables, denoted as $\boldsymbol{l}$ and $\boldsymbol{u}$, respectively.

2.2. Variable-fidelity EM simulation models

High cost of evaluating the high-fidelity model $\boldsymbol{R}_f$ makes its direct multi-objective optimization prohibitive. Computational speedup can be obtained using surrogate-assisted techniques [7,43,44], where the optimization burden is shifted into the cheaper representation of the structure of interest. In some situations, typically for simple components, development of analytical models is possible [45,46], in others (particularly for structures such as microwave filters, couplers or power splitters), equivalent circuit models can be used [1], [30]. Both types of models are very fast. Unfortunately, the only generic way of creating lower-fidelity representation that applies to all types of EM models are those obtained through coarse-discretization EM simulations [43]. The design optimization methodology presented in this work relies on such low-fidelity models, denoted here as $\boldsymbol{R}_c$. By appropriate mesh density manipulation and possible other simplifications (see, e.g., [7,22]), $\boldsymbol{R}_c$ can be made significantly (10–50 times) faster than $\boldsymbol{R}_f$ [44]. Clearly, this is achieved at the expense of some accuracy degradation. Despite this speedup, direct multi-objective optimization using population-based metaheuristics is usually too expensive even at the $\boldsymbol{R}_c$ level, and additional measures have to be taken to make the optimization process computationally feasible. One of them is construction of an even faster model using response surface approximations, specifically, kriging interpolation.

2.3. Kriging interpolation

In this section, we briefly formulate the response surface approximation (RSA) model exploited in this work, specifically, kriging interpolation [23,47]. It is utilized by the multi-objective optimization procedures of Sections 3 and 4 to generate the initial approximation of the Pareto set and its further refinement [43,44].

Let $X_B = \{\boldsymbol{x}^1, \boldsymbol{x}^2, \ldots, \boldsymbol{x}^N\}$ denote a base set, such that the responses $\boldsymbol{R}_c(\boldsymbol{x}^j)$ are known for $j = 1, 2, \ldots, N$. Let $\boldsymbol{R}_c(\boldsymbol{x}) = [R_{c.1}(\boldsymbol{x}) \ldots R_{c.m}(\boldsymbol{x})]^T$. As mentioned before, the components of the model response vector correspond to certain parameters, in particular, complex S-parameters of the structure evaluated at a discrete set of m frequency points. Here, we use ordinary kriging [23] that estimates deterministic function f as $f_p(\boldsymbol{x}) = \mu + \varepsilon(\boldsymbol{x})$, where μ is the mean of the response at base points, and ε is the error with zero expected value, and with a correlation structure being a function of a generalized distance between the base points. We use a Gaussian correlation function of the form

$$R(\boldsymbol{x}^i, \boldsymbol{x}^j) = \exp\left[\sum_{k=1}^{N} \theta_k |x_k^i - x_k^j|^2\right] \quad (1)$$

where θ_k are unknown correlation parameters used to fit the model, while $x_k{}^i$ and $x_k{}^j$ are the kth components of the base points $\boldsymbol{x}^i$ and $\boldsymbol{x}^j$.

The kriging-based coarse model $\boldsymbol{R}_s$ is defined as

$$\boldsymbol{R}_s(\boldsymbol{x}) = [R_{s.1}(\boldsymbol{x}) \ldots R_{s.m}(\boldsymbol{x})]^T \quad (2)$$

where

$$R_{s.j}(\boldsymbol{x}) = \bar{\mu}_j + \boldsymbol{r}^T(\boldsymbol{x})\boldsymbol{R}^{-1}(\boldsymbol{f}_j - \boldsymbol{1}\bar{\mu}_j) \quad (3)$$

Here $\boldsymbol{1}$ denotes an N-vector of ones,

$$\mathrm{f}_j = [R_{c.j}(\boldsymbol{x}^1) \ldots R_{c.j}(\boldsymbol{x}^N)]^T \quad (4)$$

$\boldsymbol{r}$ is the correlation vector between the point $\boldsymbol{x}$ and base points

$$\boldsymbol{r}^T(\boldsymbol{x}) = [R(\boldsymbol{x}, \boldsymbol{x}^1) \ldots R(\boldsymbol{x}, \boldsymbol{x}^N)]^T \quad (5)$$

where as $\boldsymbol{R}$ is the correlation matrix between the base points

$$\boldsymbol{R} = \left[R(\boldsymbol{x}^j, \boldsymbol{x}^k)\right]_{j,k=1,\ldots,N} \quad (6)$$

The mean $\bar{\mu}_j$ is given by $\bar{\mu}_j = (\boldsymbol{1}^T\boldsymbol{R}^{-1}\boldsymbol{1})^{-1}\boldsymbol{1}^T\boldsymbol{R}^{-1}\boldsymbol{f}_j$. The correlation parameters θ_k are found by maximizing [23]

$$-[N \ln(\bar{\sigma}^2) + \ln|\boldsymbol{R}|]/2 \quad (7)$$

in which the variance $\bar{\sigma}_j^2 = (\boldsymbol{f}_j - \boldsymbol{1}\bar{\mu}_j)^T\boldsymbol{R}^{-1}(\boldsymbol{f}_j - \boldsymbol{1}\bar{\mu}_j)/N$ and $|\boldsymbol{R}|$ are both functions of θ_k. Here, the kriging model is implemented using the DACE Toolbox [48].

2.4. Initial design space reduction

The most important advantage of the kriging interpolation surrogate $\boldsymbol{R}_s$ is its low evaluation cost. In particular, $\boldsymbol{R}_s$ can be utilized (cf. Section 2.5) for generating the initial Pareto set by means of multi-objective evolutionary optimization because the cost of such optimization can be neglected (compared to evaluation of the high-fidelity EM model) even if tens of thousands of objective evaluations are necessary. On the other hand, a serious disadvantage of approximation modeling is curse of dimensionality: the number of the training points necessary to ensure sufficient model accuracy grows very quickly with the dimensionality of the search space. Consequently, the cost of setting up the kriging model may quickly surpass the computational savings due to the entire surrogate-based multi-objective optimization procedure considered here. Also, the number of design parameters for contemporary EM simulation models tend to be large due to complexity of the respective structures. At the same time, the initial ranges for these geometry parameters are usually set rather wide to ensure that the optimum design (or, in case of multi-objective optimization, the Pareto set) is allocated within the prescribed bounds. Setting up the RSA model in such large initial spaces, particularly for large number of adjustable parameters, is virtually impractical. The initial design space reduction is therefore fundamental for successful RSA-assisted EM-driven optimization.

Fortunately, the Pareto set normally resides in a very small region of the initial design space [44]. The aim of the design space reduction procedure [44] is to limit the ranges of the parameters so that the reduced space determined by these updated parameter ranges is as small as possible yet contains possibly large portion of the Pareto front.

Let $\boldsymbol{l}$ and $\boldsymbol{u}$ be the initially defined lower/upper bounds for the design parameters. Let

$$\boldsymbol{x}_c^{*(k)} = \arg\min_{\boldsymbol{l} \leq \boldsymbol{x} \leq \boldsymbol{u}} F_k(\boldsymbol{R}_c(\boldsymbol{x})) \quad (8)$$

$k = 1, \ldots, N_{obj}$ be an optimum design of the coarse-mesh model $\boldsymbol{R}_c$ obtained with respect to the kth objective. In the second stage,

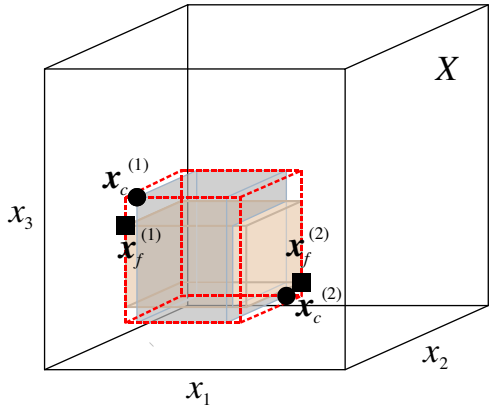

Fig. 1. Initial design space X reduction through single-objective optimization runs [44]. The extreme Pareto set points corresponding to the approximate optima of the coarse-mesh model (■) (cf. (8)) and the high-fidelity model (●) (cf. (9)) determine the reduced design space (dashed lines).

we obtain the corresponding (approximate) high-fidelity model optima

$$\boldsymbol{x}_f^{*(k)} = arg\min_{\boldsymbol{l}\le\boldsymbol{x}\le\boldsymbol{u}} F_k\left(\boldsymbol{R}_f(\boldsymbol{x})\right) \tag{9}$$

The designs $\boldsymbol{x}_f^{*(k)}$ are found using surrogate-based optimization (typically, frequency scaling combined with additive response correction is utilized [43]). The typical cost of such a process corresponds to a few evaluations of $\boldsymbol{R}_f$ [44]. The bounds of the reduced design space are then defined as (cf. Fig. 1) $\boldsymbol{l}^* = \min\{\boldsymbol{x}_{cd}^{*(1)}, \ldots, \boldsymbol{x}_{cd}^{*(N_{obj})}, \boldsymbol{x}_f^{*(1)}, \ldots, \boldsymbol{x}_f^{*(N_{obj})}\}$ and $\boldsymbol{u}^* = \max\{\boldsymbol{x}_{cd}^{*(1)}, \ldots, \boldsymbol{x}_{cd}^{*(N_{obj})}, \boldsymbol{x}_f^{*(1)}, \ldots, \boldsymbol{x}_f^{*(N_{obj})}\}$.

For typical shapes of the Pareto front, the reduced space contains both the front for the coarse-mesh and the high-fidelity and the models. The former is important because the RSA model created in $[\boldsymbol{l}^*, \boldsymbol{u}^*]$ is a representation of $\boldsymbol{R}_c$. The latter is essential to ensure sufficient room for improving the high-fidelity designs during the refinement stage (cf. Section 2.6).

2.5. Initial pareto set approximation

The initial approximation of the Pareto front is obtained by optimizing the kriging surrogate model $\boldsymbol{R}_s$ using a multi-objective evolutionary algorithm (MOEA). Here, we use a standard floating-point multi-objective evolutionary algorithm is utilized [11,49]. The algorithm is initialized using a randomly generated population. The individual assessment is based on a Pareto-dominance relation, which is utilized to rank the individuals. The dynamic fitness sharing mechanism is utilized to prevent clustering of the individuals within the solution space by penalizing the designs the are allocated too close to each other. The shared fitness of ith individual f_i is defined as [49]:

$$f_i' = \frac{f_i}{\sum_{j=1}^{P} SF^{(i,j)}} \tag{10}$$

here, f_i denotes fitness, P stands for the total number of individuals and $SF^{(i,j)}$ is the sharing function of the form

$$SF^{(i,j)} = \begin{cases} 1 - \left(\dfrac{\delta^{(i,j)}}{\sigma_r}\right) & \text{if} \delta^{(i,j)} < \sigma_r \\ 0 \quad \text{if} \delta^{(i,j)} \ge \sigma_r \end{cases} \tag{11}$$

where $\delta^{(i,j)}$ and σ_r are the Euclidean distance between ith and jth individual stands and a relation of population size to the size of Pareto front, respectively.

Generation of the new individuals is based on a Pareto-based tournament selection mechanism. Mating restrictions are also utilized to ensure that only individuals located in close proximity to each other can be crossed over. Here, the acceptable range changes dynamically and it is the same as fitness sharing radius. The probability of mutation and crossover for selected individuals is 20% and 50%, respectively. The former is realized as alterations of randomly selected components of an individual, whereas the latter is arithmetic averaging. Finally, the elitism mechanism utilized in the MOEA is aimed at preserving of currently non-dominated solutions and the offspring population. More detailed description of algorithm components can be found in [11,49].

It should be noted that because the RSA model is very fast, one can afford execution of MOEA at this stage of the process. In particular, in order to obtain a good representation of the Pareto front, we utilize a rather large population (500 individuals in the numerical experiments reported in Section 3). Nevertheless, the computational cost of MOEA optimization is normally low and corresponds to one or two evaluations of the high-fidelity EM antenna model.

Another important aspect of MOEA optimization of R_s is repeatability of the results. The variance of the obtained Pareto front representations can be greatly reduced by large population size mentioned in the previous paragraph to the extent of being practically insignificant as indicated by our numerical experiments reported in Section 3. On the other hand, one needs to remember that the initial Pareto set is subjected to the refinement process as described in Section 2.6, which further reduces its statistical variations due to MOEA optimization.

2.6. Pareto set refinement

The Pareto set obtained in Section 2.5 is merely an approximation of the true Pareto front, corresponding to the RSA model (which, in turn, is an approximation of the low-fidelity EM simulation model $\boldsymbol{R}_c$). The refinement procedure [43,44] described below aims at elevating a set of the selected designs $\boldsymbol{x}_s^{(k)}$, $k = 1, \ldots, K$, extracted from the initial Pareto set found by MOEA to the high-fidelity EM model level. The refinement stage exploits the additive response correction (output space mapping, OSM) [22,31,43] of the form:

$$\boldsymbol{x}_f^{(k.i+1)} = arg\min_{\boldsymbol{x}} F_1\left(\boldsymbol{R}_s(\boldsymbol{x}) + [\boldsymbol{R}_f(\boldsymbol{x}_s^{(k.i)}) - \boldsymbol{R}_s(\boldsymbol{x}_s^{(k.i)})]\right) \tag{12}$$

subject to

$$F_q(\boldsymbol{x}) \le F_q(\boldsymbol{x}_s^{(k.i)}),\ q=2,\ldots, N_{obj} \tag{13}$$

The optimization process (12) is constrained not to increase the remaining objectives as compared to $x_s^{(k)}$. The surrogate model R_s is corrected using the OSM term $R_f(x_s^{(k.i)}) - R_s(x_s^{(k.i)})$ (here, $x_f^{(k.0)} = x_s^{(k)}$). Consequently, the corrected surrogate coincides with R_f at the beginning of each iteration. In practice, 2 or 3 iterations of (12) are sufficient to find a refined high-fidelity model design $x_f^{(k)}$. After completing this stage, a set of Pareto-optimal high-fidelity model designs is created. This set is the final outcome of the multi-objective optimization process.

2.7. Optimization flow

The entire multi-objective design optimization algorithm can be summarized as follows [44]:

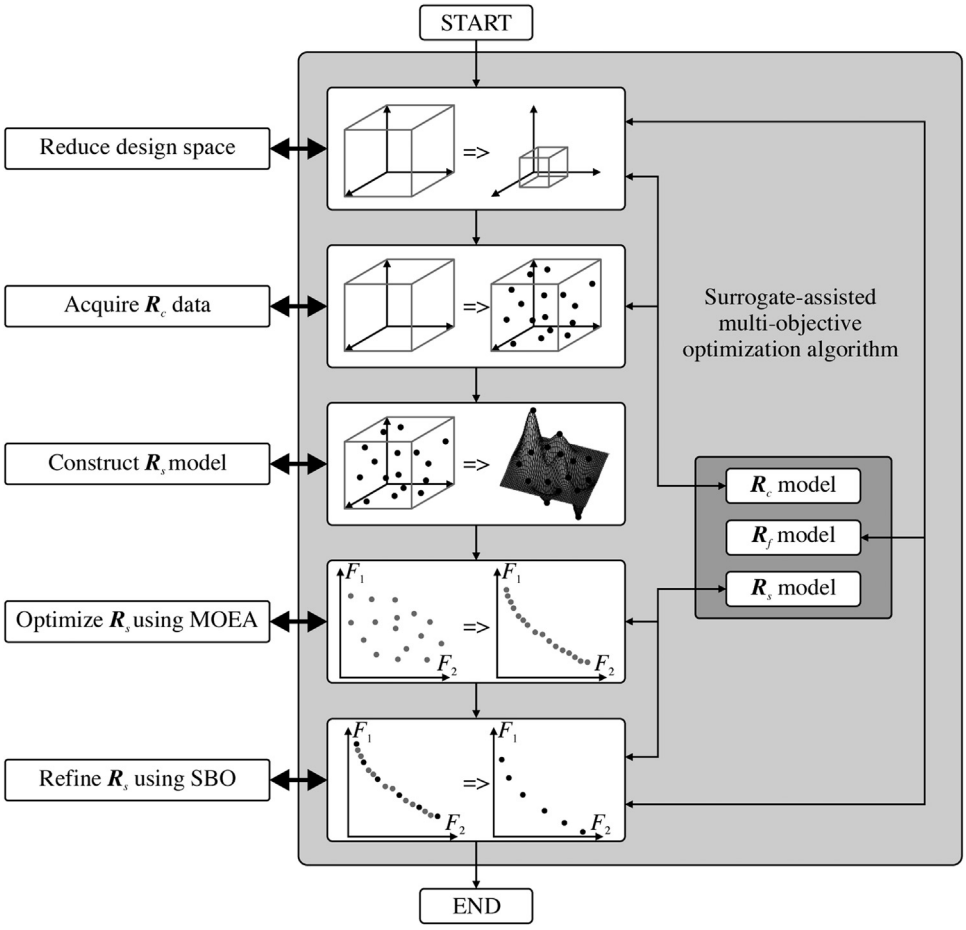

Fig. 2. Flowchart of the surrogate-assisted multi-objective antenna design optimization process.

1. Perform design space reduction (Section 2.4)
2. Sample the design space and acquire the $\boldsymbol{R}_c$ data;
3. Construct the kriging interpolation model $\boldsymbol{R}_s$ (Section 2.3);
4. Obtain the initial Pareto set by optimizing $\boldsymbol{R}_s$ using MOEA (Section 2.5);
5. Refine selected elements of the Pareto set, $\boldsymbol{x}_s^{(k)}$, to obtain the corresponding high-fidelity model designs $\boldsymbol{x}_f^{(k)}$ (Section 2.6).

It is worth noticing that the high-fidelity model $\boldsymbol{R}_f$ is not evaluated until the refinement stage (Step 5 above). Furthermore, the cost of finding the high-fidelity model Pareto-optimal set is only about three evaluations of the high-fidelity model per design and it is pretty much independent of the dimensionality of the design space. Fig. 2 shows the flow diagram of the entire optimization process.

3. Numerical studies

In this section we present three design case studies concerning a wideband impedance matching transformer (Section 3.1), a dielectric resonator antenna (Section 3.2), and an ultra-wideband monopole antenna (Section 3.3). In each case, we describe the experimental setup, numerical results, as well as the statistical analysis concerning MOEA optimization of the kriging interpolation surrogate model $\boldsymbol{R}_s$.

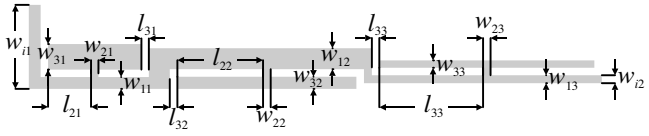

Fig. 3. Geometry of a compact 50 ohm to 130 ohm matching transformer composed of three T-shaped slow-wave resonant structure sections.

3.1. Multi-objective optimization of wideband impedance matching transformer

The first design example is a wideband microstrip matching transformer shown in Fig. 3 [50]. The circuit is composed of a cascade of three T-shaped slow-wave resonant structures and it is supposed to match the 50 ohm input to the 130 ohm load. The transformer is implemented on a 0.762 mm thick Taconic RF-35 dielectric substrate ($\varepsilon_r = 3.5$; tan $\delta = 0.0018$). The design is represented by the following 15-variable parameter vector:

$$\mathrm{x} = [w_{11}w_{21}w_{31}l_{21}l_{31}w_{12}w_{22}w_{32}l_{22}l_{32}w_{13}w_{23}w_{33}l_{23}l_{33}]^T$$

The variables in the vector $\boldsymbol{x}$ are in three groups, each of which describe one T-shaped section of the transformer. Parameters w_{mn} and l_{mn} (where m is the number of the respective parameter in a group and n denotes section number) determine the widths and the lengths of the T-shape, respectively. It should be noted that parameters $w_{i1} = 1.7$ and $w_{i2} = 0.15$ remain fixed to ensure the required source and load impedances. All parameters are in mm.

The generic design optimization procedure of Section 2 involves two EM models of the transformer. The high-fidelity model $\boldsymbol{R}_f(\boldsymbol{x})$

consists of about 1,200,000 hexahedral mesh cells and its average simulation time on a 2.1 GHz Intel Xeon CPU with 64 GB RAM is 12 min. The low-fidelity $\boldsymbol{R}_{cd}(\boldsymbol{x})$ representation of the structure contains ~55,000 cells (average simulation time: 49 s). Both models are designed in CST Microwave Studio and simulated using its time domain solver [21]. Two design objectives are considered in the optimization process: (i) $F_1(\boldsymbol{x})$ – miniaturization of the transformer footprint defined as $A \times B$ rectangle, where $A = 2\cdot(l_{21} + l_{31}) + w_{21} + w_{12} + 2\cdot(l_{22} + l_{32}) + w_{22} + w_{13} + 2\cdot(l_{23} + l_{33}) + w_{23}$ and $B = w_{11} + w_{31} + l_{31}$, as well as (ii) $F_2(\boldsymbol{x})$ – minimization of return loss over the 3.1 GHz to 10.6 GHz band of interest. The latter is defined as $\max(|S_{11}|_{3.1\text{GHzto}10.6\text{GHz}})$. The objective $F_2(\boldsymbol{x})$ is constrained to ensure that the Pareto-optimal set is composed of designs that fulfill requirements upon acceptable return loss below the threshold value $|S_t| = -10$ dB. The penalty function is given by:

$$U_2(\boldsymbol{x}) = F_2(\boldsymbol{x}) + \beta_2 \left(\max \left\{ \left| \frac{S_t - F_1\boldsymbol{x}}{S_t} \right|, 0 \right\} \right) \quad (14)$$

with the experimentally selected penalty factor $\beta_2 = 10^5$. Initial lower/upper bounds $\boldsymbol{l}/\boldsymbol{u}$ for the design variables are:

$$\mathrm{l} = [0.150.150.150.50.150.150.150.150.50.150.150.150.150.50.15]^T$$

and

$$\mathrm{u} = [1.01.01.05.00.51.01.01.05.00.51.01.01.05.00.5]^T.$$

The refined design space is obtained using procedure of Section 2.4. The obtained reduced design bounds are as follows:

$$\mathrm{l}^* = [0.240.490.860.360.150.211.730.150.160.151.80.14]^T$$

$$\mathrm{u}* = [0.390.891.660.440.160.252.330.150.170.202.320.15]^T$$

It should be noted that the dimensionality of the problem has been effectively reduced to 12 independent variables because the updated lower and upper bounds have the same values for certain parameters. In particular, the parameters $w_{21} = 0.15$, $l_{31} = 0.15$ and $w_{33} = 0.15$ became fixed according to the new bounds [44]. The final design space is 16 orders smaller than the initial one (volume-wise). In the next step, a total of 1002 training samples allocated using Latin Hypercube Sampling technique have been utilized for a construction of the kriging interpolation model $\boldsymbol{R}_s$. The cross-validation error of obtained models is 2% which is sufficient for reliable representation of circuit behavior.

Subsequently, the RSA model has been optimized using multi-objective evolutionary algorithm (cf. Section 2.5). The algorithm setup is: population size 500 and 50 generations. Next, a set of 10 designs has been selected along the obtained initial Pareto-optimal set and refined using response correction technique of Section 2.6. A comparison of the high- and the low-fidelity representation of the Pareto front is shown in Fig. 4. The frequency responses of the five refined designs are shown in Fig. 5, whereas their detailed dimensions and objective values with respect to both objectives are gathered in Table 1. It should be noted that the variability of F_1 and F_2 along the high-fidelity Pareto set is from −10 dB to −14.4 dB. The transformer size is changes from 11 mm^2 to over 19.5 mm^2 (43%).

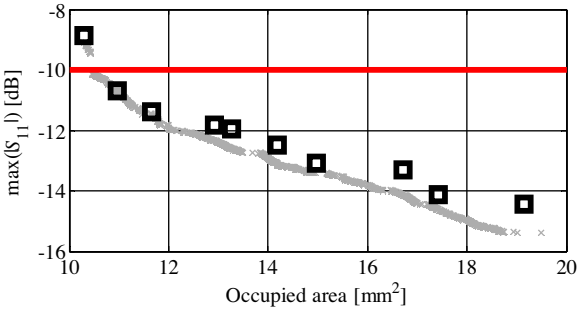

Fig. 4. Comparison of high-(□) and low-fidelity (×) representations of Pareto front.

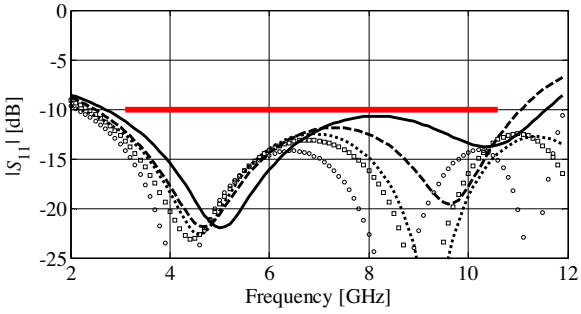

Fig. 5. Retund loss responses of selected matching transformer designs: $\boldsymbol{x}_f^{(2)}$ – (—), $\boldsymbol{x}_f^{(4)}$ – (– –), $\boldsymbol{x}_f^{(6)}$ – (···), $\boldsymbol{x}_f^{(8)}$ – (□□□), $\boldsymbol{x}_f^{(10)}$ – (○○○).

A total numerical cost of transformer optimization corresponds to 133 $\boldsymbol{R}_f$ model evaluations (~27 h) and it includes: 520 $\boldsymbol{R}_{cd}$ simulations for the design space reduction, 1000 $\boldsymbol{R}_{cd}$ evaluations during data acquisition step as well as 30 $\boldsymbol{R}_f$ simulations for the refinement of selected samples, respectively. The cost of multi-objective optimization is negligible since it is performed using the fast RSA model. The overall CPU-time required by the discussed method is significantly lower than the estimated cost of direct multi-objective optimization of the $\boldsymbol{R}_f$ model (>25,000 evaluations).

It should be noted that quality of the results obtained at the stage of initial Pareto set generation (MOEA optimization of the kriging surrogate) is not critical. The designs selected from the Pareto set are exploited as starting points and subsequently are elevated to the high-fidelity model level using SBO-based refinement algorithm.

Table 1
Three-section matching transformer optimization results.

Selected designs		$\boldsymbol{x}_f^{(2)}$	$\boldsymbol{x}_f^{(4)}$	$\boldsymbol{x}_f^{(6)}$	$\boldsymbol{x}_f^{(8)}$	$\boldsymbol{x}_f^{(10)}$
F_1 – $\lvert S_{11}\rvert$ [dB]		−10.7	−11.8	−12.5	−13.1	−14.44
F_2 – area [mm^2]		11.0	12.9	14.2	15.0	19.15
Design variables (all parameters in millimeters)	w_{11}	0.38	0.38	0.33	0.39	0.39
	w_{31}	0.50	0.57	0.71	0.84	0.77
	l_{21}	0.87	1.17	1.50	1.56	1.61
	w_{12}	0.42	0.41	0.36	0.42	0.40
	w_{22}	0.15	0.15	0.15	0.15	0.15
	w_{32}	0.25	0.22	0.22	0.21	0.23
	l_{22}	1.73	1.74	1.73	2.20	2.02
	l_{32}	0.15	0.15	0.15	0.15	0.15
	w_{13}	0.16	0.16	0.17	0.16	0.16
	w_{23}	0.15	0.15	0.16	0.17	0.17
	l_{23}	1.80	2.03	1.80	2.18	2.05
	l_{33}	0.15	0.15	0.15	0.15	0.15

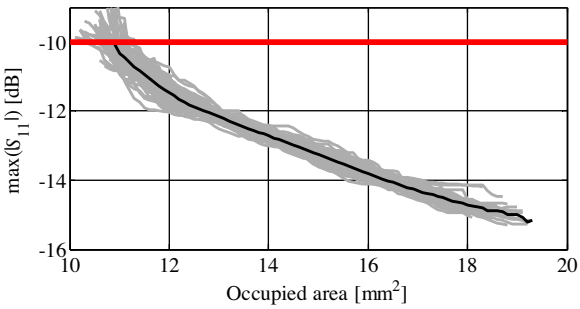

Fig. 6. The Pareto-optimal sets obtained in 50 runs of MOEA (gray lines) and the average (black line). Discrepancies between individual runs are insignificant from the engineering point of view, particularly given the range of variability for the design objectives.

Nonetheless, the outcome of the optimization process is influenced by the stochastic nature of the utilized evolutionary algorithm. For that reason a statistical analysis has been performed based on 50 runs of the MOEA routine. The results shown in Fig. 6 indicate minor variability of the Pareto front across the runs.

The largest discrepancy between the individual Pareto set and the average is around 0.7 dB which is considered negligible from the circuit operation standpoint. Moreover, the standard deviation of the results and average distance from the mean value are 0.14 dB and 0.16 dB, respectively. Consequently, the influence of the evolutionary algorithm on the refinement stage, as well as on overall results of the design optimization procedure is considered negligible.

3.2. Multi-objective optimization of quasi-isotropic dielectric resonator antenna

The next design example is a compact, quasi-isotropic dielectric resonator antenna shown in Fig. 7 [15]. The structure is implemented using a Taconic CER-10 cuboid-shape dielectric resonator ($\varepsilon_r = 10$ and $\tan\delta = 0.0035$) with a driven element in the form of a coaxial probe localized within the material. The probe is fed through a coaxial 50 ohm transmission line. The antenna is represented by a six-variable vector: $\boldsymbol{x} = [a\ b\ c\ o_1\ o_2\ l_1]^T$, whereas dimensions $d = 1.26$ and $g = 0.82$ remain fixed to ensure 50 ohm input impedance. Parameters a, b and c represent width, length and height of the dielectric resonator, respectively. Variables o_1 and o_2 denote distance of the probe with respect to center of the dielectric resonator (see Fig. 1(b)), whereas dimension l_1 represents length of the probe.

The design optimization procedure described in this work requires utilization of two antenna models (both evaluated using CST Microwave Studio). The high-fidelity $\boldsymbol{R}_f$ representation of the structure consists of 1,000,000 hexahedral mesh cells and its typical evaluation time is around 21 min. Its low-fidelity counterpart $\boldsymbol{R}_c$ is constructed using ~55,000 mesh cells (evaluation time 35 s). Three design objectives are considered: F_1–minimization of the maximum $|S_{11}|$; F_2–minimization of ΔG defined as difference between minimal and maximal E-field strength in x-z plane; F_3–minimization of antenna volume $A = a \times b \times c$. It should be noted that F_1 is considered within 2.4 GHz to 2.5 GHz frequency band, whereas F_2 is evaluated at 2.45 GHz. Moreover, only the designs that maintain return loss (objective F_1) below the acceptable level of −10 dB are of interest from the optimization standpoint.

The initial design space is defined by the following bounds: $\boldsymbol{l} = [3\ 3\ 3\ -0.45{\cdot}a\ -0.45{\cdot}b\ 0]^T$ and $\boldsymbol{u} = [30\ 30\ 20\ 0.45{\cdot}a\ 0.45{\cdot}b\ c]^T$. The linear constraints are necessary to ensure allocation of the probe within the resonator. The multi-objective optimization of the antenna is performed by following the flow described in Section 2.7. The technique of Section 2.4 is utilized to yield the reduced design bounds: $\boldsymbol{l}^* = [3.3\ 24.5\ 14.5{-}0.03{\cdot}a\ 0.37{\cdot}b\ 0.63{\cdot}c]^T$ and $\boldsymbol{u}^* = [29.8\ 30\ 15.8\ 0.16{\cdot}a\ 0.45{\cdot}b\ 0.98{\cdot}c]^T$. The reduced solution space is 10^4 smaller (volume-wise) in comparison with the initial one.

In the next step, a kriging interpolation model $\boldsymbol{R}_s$ is constructed within refined bounds using 576 low-fidelity model samples. The obtained average relative RMS error of the model—calculates using cross-validation technique [23]—is 3%. The initial Pareto front is obtained using MOEA. Algorithm setup is as follows: 2000 individuals involved in optimization process and 50 iterations.

After the optimization a set of 14 designs selected from the initial front are subjected to the refinement procedure of Section 2.6. Fig. 8 shows the initial front and the refined high-fidelity model designs. The detailed dimensions of selected Pareto optimal designs are gathered in Table 2, whereas their corresponding frequency responses and radiation patterns are shown in Fig. 9. The ranges of variability of selected high-fidelity designs with respect to F_1, F_2, and F_3 along the Pareto front are 3.2 dB, 2.8 dB and 6201 mm^3 (over 61%), respectively. It should be emphasized that significant reduction of antenna size can be obtained (from almost 11,000 mm^3 to less than 3000 mm^3). On the other hand, miniaturization influences on deterioration of the second objective ΔG (from about 5 dB to over 8 dB), which may or may not be acceptable depend-

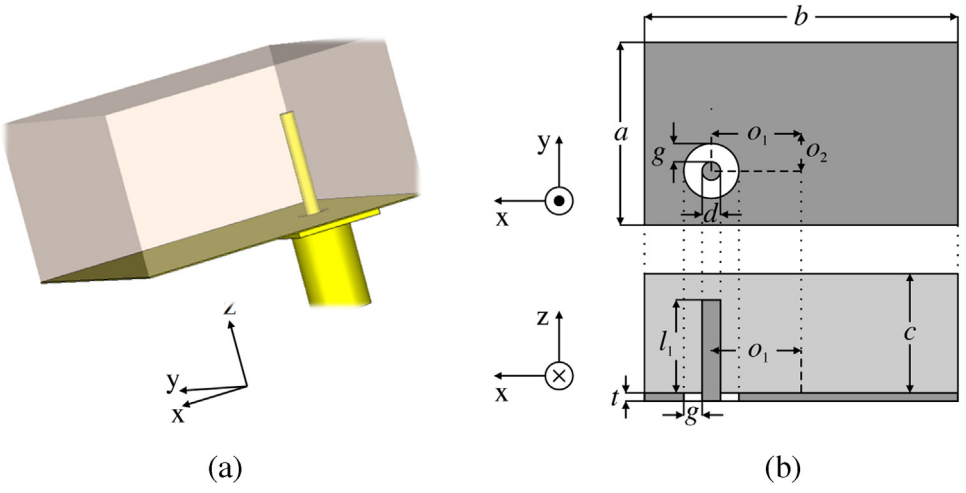

Fig. 7. Geometry of the compact DRA: (a) 3D visualization; (b) geometrical details. Light and dark gray in (b) represents dielectric resonator and metallization (copper), respectively.

Table 2
Selected Pareto-optimal designs of the DRA.

F_1[dB]	F_2[dB]	F_3[mm^3]	Design Variables [mm]					
			a	b	c	o_1	o_2	l
−10.0	5.0	9780	25.5	25.5	15.1	1.0	11.0	9.9
−10.2	5.9	6564	16.1	27.2	15.0	1.0	11.8	9.9
−10.4	6.9	4792	11.3	28.5	14.8	0.8	11.6	10.2
−11.8	7.8	3962	9.2	29.7	14.6	1.0	12.1	10.0
−13.2	5.4	10163	26.6	26.3	14.5	1.3	11.1	9.2
−12.6	6.0	7870	19.9	27.3	14.5	1.6	12.3	9.2

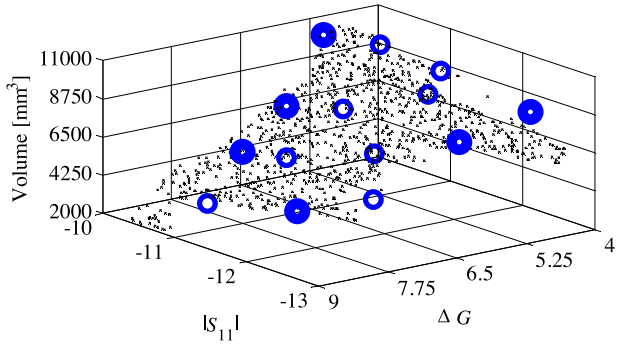

Fig. 8. The initial (×) and refined (○) Pareto set representation obtained by the multi-objective optimization procedure of Section 2. Thick-line circles denote selected designs listed in Table 2.

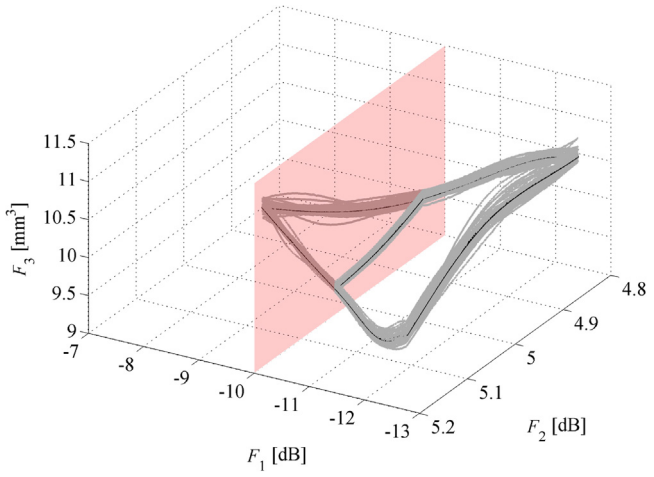

Fig. 10. Projections of the Pareto-optimal sets obtained in 50 runs of MOEA (gray lines) and the average (black line). Discrepancies between individual runs are insignificant from the engineering point of view, particularly given the range of variability for the design objectives. It should be noted that the results behind the transparent plane violate the requirements upon maximum acceptable in-band $|S_{11}|$ (assumed to be below −10 dB), so that they are of no interest.

ing on the application. Note that all designs on the Pareto front satisfy the fundamental requirement $|S_{11}| \leq -10$ dB for 2.4 GHz to 2.5 GHz band, however, for certain designs it is possible to obtain $\max|S_{11}|_{2.4\text{-}2.5\text{GHz}} \leq -13$ dB. In general, the multi-objective optimization results in a form of a Pareto set provide comprehensive information about the capabilities of the considered antenna structure.

A total cost of multi-objective antenna optimization corresponds to only about 75 $\boldsymbol{R}_f$ simulations (∼26.3 h of CPU-time) and it includes: 610 $\boldsymbol{R}_c$ simulations for design space reduction, 567 $\boldsymbol{R}_c$ evaluations for construction of the RSA model, and a total of 42 $\boldsymbol{R}_f$ simulations required for refinement of selected Pareto-optimal designs. It should be noted that estimated cost of direct multi-objective optimization of considered DRA antenna (∼100,000 $\boldsymbol{R}_f$ evaluations) is almost 4 years. Clearly, such a cost makes direct optimization computationally infeasible on a single PC machine.

The influence of the MOEA optimization step on the results of the design optimization algorithm has been verified using statistical analysis. The MOEA has been run 50 times within the refined solution space. It should be noted that the Pareto front for the three-objective case is a three-dimensional manifold so that the results of statistical analysis and their mean are shown only for selected planes (see Fig. 10 for plots). The calculated standard deviation and average distance from the mean value are 0.04 dB and 0.03 dB, respectively. At the same time, the largest discrepancy between the obtained Pareto sets and the mean within defined solution space is 0.32 dB. Such variability of the results has no meaningful influence on the structure behavior from the engineering standpoint. Consequently, the effect of the MOEA operation on the results of the discussed multi-objective optimization scheme is negligible.

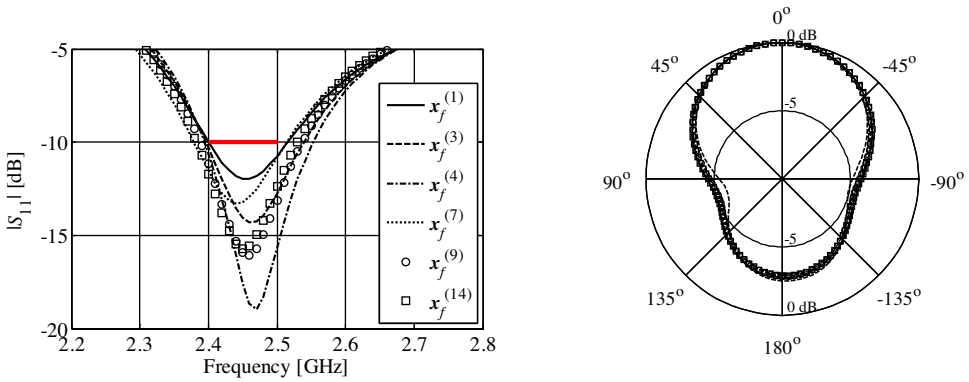

Fig. 9. Responses of selected Pareto-optimal designs of DRA antenna: (a) return loss characteristics; and (b) E-field radiation patterns in x-z plane.

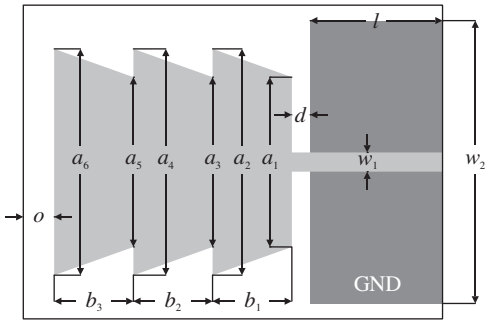

Fig. 11. Geometry of 13-variable planar UWB monopole antenna [51].

3.3. Multi-objective optimization of compact ultra-wideband monopole antenna

The last design example is 13-variable ultra-wideband (UWB) monopole antenna shown in Fig. 11. The structure is composed of a driven element in the form of three stacked trapezoids fed by a 50 ohm microstrip line [51]. The antenna is implemented on a 0.762 mm thick Taconic RF-35 dielectric substrate ($\varepsilon_r = 3.5$ tan $\delta = 0.0018$). The design is represented by the 13-variable vector: $\boldsymbol{x} = [a_1\ a_2\ a_3\ a_4\ a_5\ a_6\ b_1\ b_2\ b_3\ w_2\ l\ d\ o]^T$, whereas parameter $w_1 = 1.7$ remains fixed to ensure the 50 ohm input impedance (all dimensions are in mm). Parameters a_1–a_6 and b_1–b_3 represent width and lengths of stacked trapezoid-shape monopole radiator, whereas w_2 and l denote width and length of the substrate. Dimension d stands for a gap between the ground plane and the radiator. Finally, parameter o allows controlling offset between the radiator and substrate edge.

Both the high-fidelity model $\boldsymbol{R}_f$ and the low-fidelity model $\boldsymbol{R}_c$ are simulated in CST Microwave Studio [21]. Average evaluation time of the former is 10 min (~2,500,000 mesh cells), whereas the simulation of the latter takes 22 s (~33,600 mesh cells). The structure is to be optimized with respect to two design objectives: F_1–minimization of return loss $|S_{11}| \leq -10$ dB within 3.1–10.6 GHz frequency band of interest, and F_2–reduction of antenna footprint. The latter is defined as $A \times B$ rectangle, where $A = l + d + b_1 + b_2 + b_3 + o$ and $B = w_2 + o$.

Initial bounds for the design parameters are:

$$l = [5555551110.28.020.05.0]^T$$

and

$$u = [25.025.025.025.025.025.015.015.015.02.015.040.010.0]^T.$$

The design optimization procedure follows the general flow of Section 2.7, whereas solution space is reduced using technique of Section 2.4. The refined solution space obtained based on dimensions of the extreme designs is represented by the following bounds:

$$l = [10.0721.6322.221.020.822.73.23.812.320.578.322.075.0]^T$$

and

$$u = [11.321.9624.3024.1521.2724.63.94.013.080.7411.239.355.75]^T$$

The refined space is 14 orders of magnitude smaller (volume-wise) than the initial one. Moreover, the ranges for most of the parameters are notably flattened [44].

The kriging interpolation model $\boldsymbol{R}_s$ is generated using a total of 1500 $\boldsymbol{R}_c$ training samples. Subsequently, the obtained RSA model has been utilized as an evaluation engine for MOEA optimization. The high-fidelity representation consisting of 10 designs has been found using the refinement procedure described in Section 2.6 (cf. (12)). The minimum antenna footprint that satisfies the requirements upon return loss is 1134 mm^2. At the same time, the minimum in-band $|S_{11}|$ is only −14.9 dB. Moreover, the minimum size of the antenna, which satisfies requirements upon return loss, is almost 20% smaller than the structure optimized with respect to $|S_{11}|$. Fig. 12 shows the Pareto sets of the low- and high-fidelity models, whereas detailed dimensions of the selected designs are gathered in Table 3.

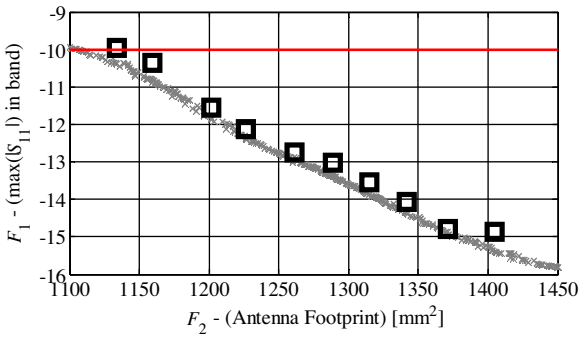

Fig. 12. The high- (□) and low-fidelity (×) representations of the Pareto front obtained using the discussed multi-objective optimization procedure.

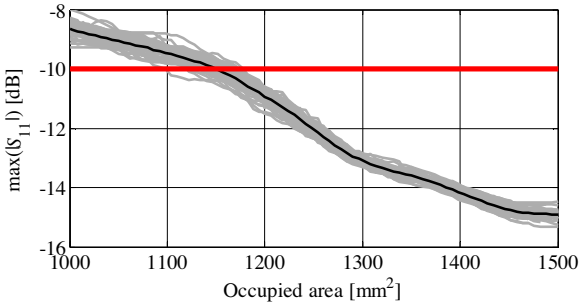

Fig. 13. The Pareto-optimal sets obtained in 50 runs of MOEA (gray lines) and the average (black line). Note minor discrepancies between consecutive runs and the mean value that are negligible from the engineering point of view.

The total computational cost of multi-objective design of the considered UWB monopole antenna corresponds to about 122 evaluations of the high-fidelity model (~20.4 h of the CPU time). The cost includes: 800 $\boldsymbol{R}_c$ and 4 $\boldsymbol{R}_f$ evaluations for the design space reduction, 1500 $\boldsymbol{R}_c$ samples acquired to form the training set for identification of the RSA model, and 30 $\boldsymbol{R}_f$ evaluations for the refinement of the 10 selected antenna designs. The above cost is negligible compared to the estimated CPU-time required by 25000 evaluations during direct MOEA optimization of the high-fidelity model $\boldsymbol{R}_f$.

Statistical analysis has been performed, in order to verify impact of the MOEA step on the final results of the design optimization algorithm. The results have been obtained based on fifty runs of MOEA within refined solution space (see Fig. 13 for plots of the fronts and mean). The largest discrepancy between the Pareto sets and the mean value is around 0.55 dB, whereas corresponding standard deviation and average distance from the mean are 0.1 dB and 0.14 dB, respectively. It should be noted that such level of variability is negligible from engineering standpoint. Consequently, it has no meaningful influence on the outcome of the design procedure of Section 2.

4. Discussion and conclusion

In the paper, we investigated cost-efficient design optimization of expensive computational electromagnetic (EM) models. We demonstrated that a suitable combination of various con-

Table 3
Optimization results of the UWB monopole antenna.

		Antenna designs									
		$\boldsymbol{x}_f^{(1)}$	$\boldsymbol{x}_f^{(2)}$	$\boldsymbol{x}_f^{(3)}$	$\boldsymbol{x}_f^{(4)}$	$\boldsymbol{x}_f^{(5)}$	$\boldsymbol{x}_f^{(6)}$	$\boldsymbol{x}_f^{(7)}$	$\boldsymbol{x}_f^{(8)}$	$\boldsymbol{x}_f^{(9)}$	$\boldsymbol{x}_f^{(10)}$
	F_1 [dB]	−10.0	−10.4	−11.0	−12.1	−12.7	−13.5	−14.1	−14.8	−14.9	−15.2
	F_2 [mm^2]	1134	1159	1185	1226	1261	1315	1342	1371	1405	1475
Antenna Parameters	a_1	10.07	10.09	10.38	11.06	11.11	11.14	11.11	10.95	10.97	10.90
	a_2	21.63	21.68	21.69	21.69	21.70	21.94	21.91	21.82	21.76	21.77
	a_3	22.20	22.20	22.20	22.20	22.20	22.20	22.20	22.23	22.20	22.38
	a_4	21.00	21.00	21.00	21.00	21.32	21.36	21.64	22.00	22.79	22.44
	a_5	20.80	20.87	20.98	21.02	21.04	20.93	20.94	20.92	21.01	20.88
	a_6	22.70	22.70	23.12	24.25	24.07	24.15	23.80	24.28	23.70	24.07
	b_1	3.90	3.90	3.87	3.54	3.64	3.83	3.86	3.88	3.90	3.89
	b_2	3.80	3.80	3.80	3.80	3.89	3.95	3.93	3.99	3.92	3.99
	b_3	12.32	12.32	12.32	12.32	12.38	12.62	12.72	13.01	13.02	13.08
	w_2	0.60	0.60	0.61	0.61	0.62	0.64	0.65	0.63	0.67	0.65
	l	11.15	11.15	11.12	11.04	11.05	10.82	10.74	10.62	10.60	10.59
	d	28.34	29.03	29.77	31.28	31.99	33.18	33.87	34.40	35.35	37.00
	o	5.00	5.00	5.00	5.00	5.00	5.00	5.00	5.02	5.00	5.09

cepts borrowed from surrogate-based modeling and optimization such as utilization of variable-fidelity EM simulations, response correction techniques, as well as response surface approximation modeling, allows for expedited identification of Pareto-optimal designs at the cost corresponding to just a few dozen of high-fidelity EM model evaluations. Our methodology can be applied in various fields exploiting computational electromagnetics such as microwave and antenna engineering, wireless power transfer, microwave photonics, etc. We discussed several specific applications, including multi-objective design of a wideband impedance matching transformer and two antenna structures. A potentially high cost of evolutionary-algorithm-based optimization required to identify the Pareto front has been mitigated by executing the search at the level of a fast kriging interpolation model and subsequent Pareto set refinement (also realized with surrogate-based optimization). Design space reduction applied as the first stage of the process allows for handling higher-dimensional problems. Also, suitable statistical studies demonstrated that the potential issue of lack of repeatability of Pareto front identification with population-based metaheuristics is well controlled by the remaining stages of the optimization process. Overall, the framework discussed in this work may be considered as a step towards computationally-efficient automation of multi-objective design optimization processes involving expensive simulation models. Although showcased for problems in computational electromagnetics, it might also be useful for handling design tasks in other engineering fields.

Acknowledgements

The authors would like to thank Computer Simulation Technology AG, Darmstadt, Germany, for making CST Microwave Studio available. This work was supported in part by the Icelandic Centre for Research (RANNIS) Grants 1502034051 and 163299051, and by National Science Centre of Poland Grant 2013/11/B/ST7/04325.

References

[1] P. Kurgan, A. Bekasiewicz, M. Pietras, M. Kitlinski, Novel topology of compact coplanar waveguide resonant cell low-pass filter, Microw. Opt. Technol. Lett. 54 (3) (2012) 732–735.
[2] M. Bod, H.R. Hassani, M.M.S. Taheri, Compact UWB printed slot antenna with extra bluetooth, GSM, and GPS band, IEEE Antennas Wirel. Propag. Lett. 11 (2012) 531–534.
[3] S. Koziel, S. Ogurtsov, Fast surrogate-assisted simulation-driven optimisation of add-drop resonators for integrated photonic circuits, IET Microw., Antennas Propag. 9 (7) (2015) 672–675.
[4] A. Costanzo, M. Dionigi, D. Masotti, M. Mongiardo, G. Monti, L. Tarricone, R. Sorrentino, Electromagnetic energy harvesting and wireless power transmission: a unified approach, Proc. IEEE 102 (no. 11) (2014) 1692–1711.
[5] K. Moussakhani, R.K. Amineh, N.K. Nikolova, Estimating the efficiency of antennas used as sensors in microwave tissue measurements, IEEE Trans. Antennas Propag. 62 (no. 1) (2014) 295–301.
[6] Y. Gotoh, A. Kiya, N. Takahashi, Electromagnetic inspection of outer side defect on steel tube with steel support using 3-D nonlinear FEM considering non-uniform permeability and conductivity, IEEE Trans. Magn. 46 (no. 8) (2010) 3145–3148.
[7] A. Bekasiewicz, S. Koziel, Structure and computationally-efficient simulation-driven design of compact UWB monopole antenna, IEEE Antennas Wirel. Propag. Lett. 14 (2015) 1282–1285.
[8] S. Koziel, A. Bekasiewicz, Variable-fidelity optimization of antennas using adjoint sensitivities, in: Loughborough Antennas & Propagation Conference, Loughborough, 2014, pp. 412–415.
[9] J. Nocedal, S. Wright, Numerical Optimization, 2nd ed., Springer, New York, 2006.
[10] A. Conn, K. Scheinberg, L.N. Vincente, Introduction to derivative-Free optimization, MPS-SIAM Series Optim. (2009), Philadelphia.
[11] K. Deb, Multi-Objective Optimization Using Evolutionary Algorithms, Wiley, New York, NY, USA, 2001.
[12] N. Jin, Y. Rahmat-Samii, Advances in particle swarm optimization for antenna designs: real-number, binary, single-objective and multiobjective implementations, IEEE Tran. Antennas Propag. 55 (no. 3) (2007) 556–567.
[13] W. Wang, S. Gong, X. Wang, Y. Guan, W. Jiang, Differential evolution algorithm and method of moments for the design of low-RCS antenna, IEEE Antennas Wirel. Propag. Lett. 9 (2010) 295–298.
[14] X. Qing, Z.N. Chen, Compact coplanar waveguide-fed ultra-wideband monopole-like slot antenna, IET Microw. Antennas Propag. 3 (no. 5) (2009) 889–898.
[15] Y.-M. Pan, K.W. Leung, K. Lu, Compact quasi-isotropic dielectric resonator antenna with small ground plane, IEEE Trans. Antennas Propag. 62 (no. 2) (2014) 577–585.
[16] P.A.W. Basl, M.H. Bakr, N.K. Nikolova, Theory of self-adjoint S-parameter sensitivities for lossless nonhomogeneous transmission-line modeling problems, IET Microw. Antennas Propag. 2 (April (no. 3)) (2008) 211–220.
[17] M.H. Bakr, N.K. Nikolova, An adjoint variable method for time domain TLM with wideband Johns matrix boundaries, IEEE Trans. Microw. Theory Tech. 52 (February (no. 2)) (2004) 78–685.
[18] S. Koziel, A. Bekasiewicz, Fast EM−driven size reduction of antenna structures by means of adjoint sensitivities and trust regions, IEEE Antennas Wirel. Propag. Lett. 14 (2015) 1681–1684.
[19] A. Bekasiewicz, S. Koziel, Efficient multi-fidelity design optimization of microwave filters using adjoint sensitivity, Int. J. RF Microw. Comput. Aided Eng. 25 (no. 2) (2015) 178–183.
[20] Ansys HFSS, ver. 14.0 (2012), ANSYS, Inc., Southpointe 275 Technology Dr., Canonsburg, PA.
[21] CST. Microwave Studio, ver. 2014, CST AG, Bad Nauheimer Str. 19, D-64289 Darmstadt, Germany, 2014.
[22] Computational optimization, methods and algorithms, in: S. Koziel, X.S. Yang (Eds.), Series: Studies in Computational Intelligence, 356, Springer, 2011.
[23] N.V. Queipo, R.T. Haftka, W. Shyy, T. Goel, R. Vaidynathan, P.K. Tucker, Surrogate-based analysis and optimization, Prog. Aerosp. Sci. 41 (1) (Jan. 2005) 1–28.
[24] A.I.J. Forrester, A.J. Keane, Recent advances in surrogate-based optimization, Prog. Aerosp. Sci. 45 (2009) 50–79.
[25] Y. Jin, Surrogate-assisted evolutionary computation: recent advances and future challenges, Swarm Evol. Comput. 1 (2) (2011) 61–70.
[26] F.J. Villegas, T. Cwik, Y. Rahmat-Samii, M. Manteghi, A parallel electromagnetic genetic-algorithm optimization (EGO) application for patch antenna design, IEEE Trans. Antennas Propag. 52 (no. 9) (2004) 2424–2435.

[27] J. Knowles, ParEGO: a hybrid algorithm with on-line landscape approximation for expensive multiobjective optimization problems, IEEE Trans. Evolut. Comput. 10 (no. 1) (2006) 50–66.
[28] Y.-S. Ong, P.B. Nair, K.Y. Lum, Max-min surrogate-assisted evolutionary algorithm for robust design, IEEE Trans. Evolut. Comput. 10 (no. 4) (2006) 392–404.
[29] B. Liu, Q. Zhang, G.G.E. Gielen, A Gaussian process surrogate model assisted evolutionary algorithm for medium scale expensive optimization problems, IEEE Trans. Evol. Comput. 18 (no. 2) (2014) 180–192.
[30] A. Bekasiewicz, P. Kurgan, M. Kitlinski, A new approach to a fast and accurate design of microwave circuits with complex topologies, IET Microw. Antennas Propag. 6 (no. 14) (2012) 1616–1622.
[31] J.W. Bandler, Q.S. Cheng, S.A. Dakroury, A.S. Mohamed, M.H. Bakr, K. Madsen, J. Søndergaard, Space mapping: the state of the art, IEEE Trans. Microw. Theory Tech. 52 (no. 1) (2004) 337–361.
[32] S. Koziel, J.W. Bandler, Space mapping with multiple coarse models for optimization of microwave components, IEEE Microw. Wirel. Compon. Lett. 18 (2008) 1–3.
[33] S. Koziel, J.W. Bandler, K. Madsen, Space mapping with adaptive response correction for microwave design optimization, IEEE Trans. Microw. Theory Tech. 57 (no. 2) (2009) 478–486.
[34] S. Koziel, S. Ogurtsov, S. Szczepanski, Rapid antenna design optimization using shape-preserving response prediction, Bull. Polish Acad. Sci. Tech. Sci. 60 (no. 1) (2012) 143–149.
[35] S. Koziel, L. Leifsson, Multi-point response correction for reduced-cost EM-simulation-driven design of antenna structures, Microw. Opt. Tech. Lett. 55 (no. 9) (2013) 2070–2074.
[36] S. Koziel, J.W. Bandler, Rapid yield estimation and optimization of microwave structures exploiting feature-based statistical analysis, IEEE Trans. Microw. Theory Tech. 63 (no. 1) (2015) 107–114.
[37] S. Koziel, Adaptively adjusted design specifications for efficient optimization of microwave structures, Progress Electromagn. Res. B 21 (2010) 219–234.
[38] B. Mun, C. Jung, M.-J. Park, B. Lee, A compact frequency-reconfigurable multiband LTE MIMO antenna for laptop applications, IEEE Antennas Wirel. Propag. Lett. 13 (2014) 1389–1392.
[39] N. Chahat, M. Zhadobov, R. Sauleau, K. Ito, A compact UWB antenna for on-body applications, IEEE Trans. Antenna Propag. 59 (no. 4) (2011) 1123–1131.
[40] Y. Kuwahara, Multiobjective optimization design of Yagi–Uda antenna, IEEE Tran. Antennas Propag. 53 (June (no. 6)) (2005) 1984–1992.
[41] S. Chamaani, M.S. Abrishamian, S.A. Mirtaheri, Time-domain design of UWB Vivaldi antenna array using multiobjective particle swarm optimization, IEEE Antennas Wirel. Prop. Lett. 9 (2010) 666–669.
[42] D.R.B. de Araújo, C.J.A. Bastos-Filho, J.F. Martins-Filho, An evolutionary approach with surrogate models and network science concepts to design optical networks, Eng. Appl. Artif. Intell. 43 (2015) 67–80.
[43] S. Koziel, S. Ogurtsov, Multi-objective design of antennas using variable-fidelity simulations and surrogate models, IEEE Trans. Antennas Propag. 61 (no. 12) (2013) 5931–5939.
[44] S. Koziel, A. Bekasiewicz, W. Zieniutycz, Expedite EM-driven multi-objective antenna design in highly-dimensional parameter spaces, IEEE Antennas Wirel. Propag. Lett. 13 (2014) 631–634.
[45] B. Aljibouri, E.G. Lim, H. Evans, A. Sambell, Multiobjective genetic algorithm approach for a dual-feed circular polarised patch antenna design, Electron. Lett. 36 (2000) 1005–1006.
[46] B. Aljibouri, A. Sambell, B.S. Sharif, Application of genetic algorithm to design of sequentially rotated circularly polarised dual-feed microstrip patch antenna array, Electron. Lett. 44 (2008) 708–709.
[47] J. Kleijnen, Design and Analysis of Simulation Experiments, Springer, 2008.
[48] S.N. Lophaven, H.B. Nielsen, J. Søndergaard, DACE: a Matlab Kriging Toolbox, Technical University of Denmark, 2002.
[49] C.A. Coello Coello, G.B. Lamont, D.A. Van Veldhuizen, Evolutionary Algorithms for Solving Multi-objective Problems, 2nd ed., Springer-Verlag, New York, 2007.
[50] P. Kurgan, A. Bekasiewicz, M. Kitlinski, On the low-cost design of abbreviated multi-section planar matching transformer, Microw. Opt. Technol. Lett. 57 (3) (2015) 521–525.
[51] X.-S. Yang, K.-T. Ng, S.H. Yeung, K.F. Man, Jumping genes multiobjective optimization scheme for planar monopole ultrawideband antenna, IEEE Trans. Antennas Propag. 56 (no. 12) (2008) 3659–3666.